ELEVENTH EUROPEAN ROTORCRAFT FORUM

Paper No. 7

ON HELICOPTER ROTOR LOW FREQUENCY BROADBAND NOISE

Morgan Williams
Rocketdyne Company
Canoga Park, California USA

and

Wesley L. Harris
Massachusetts Institute of Technology
Cambridge, Massachusetts USA

September 10-13, 1985
London, England UK

The City University, London, EC1V OHB, England

ON HELICOPTER ROTOR LOW FREQUENCY BROADBAND NOISE

Morgan Williams
Rocketdyne Company
Canoga Park, California USA

and

Wesley L. Harris
Massachusetts Institute of Technology
Cambridge, Massachusetts USA

ABSTRACT

The problem of helicopter low frequency broadband noise due to inflow turbulence, which is initially of shear layer type, is examined experimentally. An experiment is carried out to understand the effects of incident turbulence and rotor performance parameters on rotor low frequency broadband noise. The general methodology consisted of placing an airfoil upstream of the rotor, measuring the airfoil wake properties, and then operating the rotor in the wake of the upstream airfoil and measuring the resultant noise. The turbulence measurements indicate that initially, the inflow turbulence into the model rotor is nonisotropic. Comparison of the acoustic measurements and a noise prediction scheme which assumes the inflow turbulence to be isotropic, suggests that the initial nonisotropy of rotor inflow turbulence does not invalidate the assumption of isotropic inflow turbulence. For a variety of upstream conditions, the effect of rotor blade tip Mach number on the peak sound pressure level, was observed to be consistent with a sixth power Mach number scaling law. The experimental data also indicate that a high advance ratios, the rotor advance ratio has no strong effect on the measured peak sound pressure level. The data shows that the rotor mean loading strongly influences the measured sound pressure levels.

NOMENCLATURE

a	ambient speed of sound
b	rotor blade span
c	blade chord
c^*	characteristic length of bluff body
C_T/σ	ratio of rotor mean thrust coefficient to rotor solidity
$E(k)$	turbulence energy spectrum function
f	frequency
$F(k_x,k_z)$	Mugridge's strip theory gust function
J_0,J_1	Bessel functions of zero and first order, respectively
$\vec{k},k_i,(k_x,k_y,k_z)$	wave number vector
$K(k_x,k_z)$	unsteady lift gust response function
L	turbulence integral length scale in the longitudinal direction
M	Mach number
Q	magnitude of the blade velocity
Re	Reynolds number
R_{ij}	turbulence correlation tensor, $= \overline{U_i U_j}$
$S_{pp}^{(0)}$	sound pressure spectral density calculated using an isotropic turbulence spectrum
Ψ	rotor azimuth angle
ω_{pk}	acoustic frequency at peak sound pressure level
τ	separation time
ϕ_{uu}	one-dimensional energy spectral density for u
R_{uu}	autocorrelation of the u-velocity fluctuations
ω	observed radian acoustic frequency
S_{LL}	lift spectral density
Φ_{vv}	turbulence upwash spectral density tensor
S	Sears function

1. INTRODUCTION

Broadband noise is the sound generated by random rotor blade load fluctuations due to inflow turbulence, vortex shedding or boundary layers. Low frequency broadband noise is characterized by a continuous frequency spectrum (as opposed to impulsive or harmonic type spectra) and is devoid of any spectral humps occurring at high frequencies. The classification of rotor noise is qualitatively indicated in Aravamudan and Harris [1].

Because the broadband noise regime begins at roughly ten times the fundamental rotational frequency of the rotor, the broadband noise is usually masked by the more dominant impulsive and rotational rotor noise phenomena. However, under certain situations (e.g. forward flight), broadband noise dominates the radiated acoustics. Obviously, the design of quiet rotors requires the broadband noise mechanism to be understood.

Rotor broadband noise is an aeroacoustic phenomenon. Because of the experimental observation that the radiated sound pressure spectral densities due to broadband noise are smooth or continuous, the aeroacoustic mechanism is assumed to be random. That is why turbulence is postulated as being the mechanism for broadband noise generation. This incident turbulence can be generated by the rotor itself, e.g., shed vorticity, or the turbulence can be introduced from outside, for example, atmospheric inflow turbulence. The issue is the relationship between the incident turbulence and the radiated broadband noise.

Several M.I.T. investigators have done work in the turbulence induced rotor acoustics field. Aravamudan and Harris [1] used a biplanar grid system to generate isotropic (perfect chaos) inflow turbulence and examined the relationship between the turbulence and the radiated broadband noise of a model helicopter rotor. A number of scaling laws which correlated the turbulence and noise were developed. Humbad and Harris [2] investigated the effect of tip shape and rotor performance parameters on the noise due to inflow turbulence. Their experiments were also done on a model rotor. In addition to other interesting observations, they noted that the blade loading and inflow turbulence intensity influenced the radiated noise.

Paterson and Amiet [3] performed a comprehensive series of tests on turbulence ingestion noise for a model helicopter rotor. Using a methodology similar to Aravamudan and Harris [1], they measured the inflow properties of grid generated turbulence, and the radiated noise.

The analysis of broadband noise due to turbulence began with the theory of Homicz and George [4]. They essentially represented the rotor blades as fluctuating point forces, rotating in a circle. The fluctuating loads were related to the inflow turbulence by using unsteady airfoil theory and an isotropic turbulence spectrum. A high frequency extension of this theory was developed by George and Kim [5].

Amiet [6] approximated the noise radiation from rotating motions by averaging the radiation from a series of straight line blade motions which

approximate the actual rotor trajectory. The fluctuating blade loads were calculated by using unsteady airfoil theory and an isotropic turbulence spectrum.

These theories or noise prediction schemes, couple the inflow turbulence statistics (intensity, length scale, and energy spectral density) with unsteady airfoil theory to predict the fluctuating blade forces, and hence, the radiated noise. Using an isotropic and homogeneous turbulence assumption, these schemes have been found to be accurate (see George and Chou [7]) when compared to experimental results obtained for rotors encountering grid generated turbulence and even for full scale rotors encountering atmospheric turbulence. This is a surprising result since the local, blade incident turbulence is unlikely to be isotropic or homogeneous.

In the present investigation, shear layer inflow turbulence is generated by airfoils placed upstream of a model helicopter rotor. Three different airfoils are used. This type of inflow turbulence is initially nonisotropic. The turbulence properties of the upstream airfoil wake are measured, with the rotor nonoperative. After these measurements are taken, the rotor is operated in the airfoil wake, and the radiated noise is measured.

The measurement technique defines only the initial state of the inflow turbulence. Another technique would be to measure the blade incident turbulence and to measure the acoustics simultaneously. However the only information which can be extracted from data taken this way is fluctuating velocity histories and its correlation with the acoustics. This type of data would be nonstationary and nonhomogeneous, and a totally adequate methodology doesn't exist as yet for the analysis of all types of nonstationary data (Bendat and Piersol [8]). Therefore, to use this type of data, some assumptions must be made to allow for any type of spectral analysis. These assumptions would probably be just as artificial as current assumptions presently being made in the helicopter acoustics field, e.g., homogeneous and isotropic inflow turbulence. Also, the crucial turbulence information needed, three-dimensional wavenumber spectra, presently can't be measured even for simple flow situations.

In the present experiment, the inflow turbulence is initially, nonisotropic. It is examined how the radiated noise correlates with the type of inflow turbulence and rotor performance parameters. The validity of the isotropic turbulence assumption used in many noise prediction schemes is also investigated.

2. EXPERIMENTAL EQUIPMENT

2.1 M.I.T. Anechoic Wind Tunnel Facility

The MIT Anechoic Wind Tunnel Facility was used for the present experiment. The tunnel has a 152 by 229 cm open jet test section which is enclosed in a 366 by 366 by 732 cm anechoic chamber. The sides of the chamber are covered with Cremer blocks and the floor is covered with 15 cm thick polyurethene foam. The anechoic cut-off frequency is 160 Hz. The maximum flow Mach number for this wind tunnel is 0.10.

2.2 The Model Rotor System

The model rotor system consits of a Lebow slip ring, a thrust measuring dynamometer, a hydraulic pump and motor system, and a 127 cm rotor with fiberglass and wood blades. The blades have a span of 56 cm, a 5 cm chord and 8 degrees washout. The rotor was operated in the inverted thrust mode. See the report by Widnall, Harris, Lee and Drees [9] for more details.

2.3 Upstream Airfoils

The airfoils used to generate rotor inflow turbulence were constructed out of extruded polystyrene foam and fiberglass. The airfoils were mounted in the tunnel throat, 157 cm from the rotor centerline (measured from airfoil trailing edge), and near the rotor plane. The airfoil angle of attack was changed by rotating the airfoil about a point near the airfoil trailing edge. The NACA 0012 airfoil with a 30.5 cm chord had some residual curvature which effectively changed the trailing flow angle of attack by minus three degrees. Also, this particular airfoil had a trailing edge thickness of 0.25 cm. These characteristics do not effect the results since the velocity measurements are taken which define the flow field. Table 2-1 lists the airfoils used in the experiment.

2.4 Turbulence Instrumentation

Velocity fluctuation in the upstream airfoil wake were measured with a pair of DISA 55D05 constant temperature anemometers in conjunction with DISA 55D15 linearizers. The linearizers were calibrated to known flow velocities in the wind tunnel. An overheat ratio of 0.3 to 0.4, a linearizer exponent of 3, and a dynamic input range of 59% yielded linear calibration curves. Root mean square (rms) turbulence velocities were measured real time with a Hewlett Packard (HP) 3400A rums voltmeter, and were also calculated off-line using recorded velocity signals and a Nicolet spectrum analyzer. In cases of disagreement between real time and off-line rms results, the real time measurements were taken to be the more reliable of the two since the tape recorder added an amount of uncertainty into the recorded measurements.

The hot wire used was a DISA 55P61 cross-probe. The probe wire was a five micron platinum-rhodium (10%). The sensing portions were less than 0.13 cm long. The traversing mechanism consisted of clamps and a cylindrical rod which was attached to the wind tunnel microphone rack.

A sum and difference circuit was used to obtain longitudinal (u) and vertical (v) velocity fluctuations. These signals were stored on an Ampex FR-1300 FM recorder. A tape speed of 76 cm per second was used. All spectrum analysis and correlations were performed with a Nicolet 660B spectrum analyzer set for summation averaging over 20 - 50 preset spectra or time windows.

2.5 Acoustic Instrumentation

A 1.27 cm Bruel and Kjaer (B&K) 4133 microphone, in conjunction with a B&K 2604 amplifier, were used to measure the rotor acoustics. Measurements

were taken with the amplifier in the linear weighting mode and the fast rms meter mode. A B&K 4220 piston phone was used to calibrate the acoustic instruments. A Kruhn-Hite 335 high pass filter (160 Hz cut-off) was used to filter out the portions of the acoustic signal below the anechoic cut-off frequency. The measured acoustic pressure fluctuations were stored on the Ampex recorder and anlyzed with the Nicolet 660B. Tape recorder errors consisted of harmonic distortion (1.9%), flutter (0.6%) and random signal to noise contamination.

3. MEASUREMENT

Measurements were taken to understand the effects of type of incident turbulence, rotor advance ratio, tip Mach number and blade mean loading on rotor low frequency broadband noise. The general methodology consisted of placing an airfoil upstream of the rotor, measuring the airfoil wake properties at various freestream speeds (with the rotor nonoperative), and then operating the rotor in the wake of the upstream airfoil and measuring the resultant noise. The turbulence measurements define the initial turbulence velocity field which is uncontaminated by the rotor aerodynamics. A test matrix is presented in Table 3-1.

3.1 Comments on the Rationale of Measurement Technique

The turbulence measurements were taken with the rotor nonoperative. A question then arises, when the rotor is operated in the airfoil wake, doesn't the basic wake-rotor flow change as well as the turbulent flow? The answer is yes. This is precisely the nature of the aeroacoustic problem. One solution would be to measure the local incident velocity fluctuations on the rotor blades. But again, to draw conclusions from this type of data, some assumptions must be made since the random fields measured in this way will be both nonstationary and nonhomogeneous. And care must be taken to account for rotor aerodynamics and structural vibration contamination of the measured velocities.

From the physics of the flow situation, it is obvious that the local blade incident velocity fluctuations are a function of the initial turbulence state. Therefore, measurement of the initial turbulence state provides a logical starting point for the analysis of rotor-inflow turbulence interaction noise.

3.2 Freestream Turbulence

To ascertain the amount of turbulence in the wind tunnel without any flow obstructions (upstream airfoils) in place, freestream turbulence velocity intensities u' and v' were measured at the center of the wind tunnel test section. Figure 3-1 shows the relative freestream turbulence intensities as a function of Reynolds number based on the tunnel test section length. As the Reynolds number is increased, by increasing the tunnel flow velocity, the turbulence velocities increase but the relative turbulence intensities exhibit a noticeable decrease. Not all of the increased flow energy available from increased tunnel velocities is converted to increased turbulence production in a one-to-one fashion.

The freestream length scales were computed from the velocity autocorrelation and energy spectral density curves, and Eqs. (3.1) and (3.2). From Hinze [10],

$$\lambda = \lim_{\tau \to 0} \bar{U} \left\{ \frac{\tau^2}{1-R_{uu}(\tau)} \right\}^{1/2}, \tag{3.1}$$

and

$$L = \frac{\bar{U}}{4u'^2} \lim_{f \to 0} \phi_{uu}(f), \tag{3.2}$$

The Taylor microscale is related to eddies which produce the most rapid fluctuations in u(t). Figure 3-2 shows the variation of the turbulence length scales with Reynolds number (based on tunnel test section length). The increase in length scale with Reynolds number indicates that the one-dimensional energy spectra remain relatively unchanged as the Reynolds number increases. Figure 3-3 shows a typical autocorrelation curve and one-dimensional energy density curve. The energy spectral density was calculated with the Nicolet spectrum analyzer set for a frequency range of 10,000 Hz. The rise in spectral energy which occurs at the higher frequencies is assumed to be due to extraneous electrical noise.

3.3 Upstream Airfoil Wake Turbulence

Three airfoils were used to generate seven different states of rotor inflow turbulence. The geometry of each airfoil arrangement with respect to the rotor plane is illustrated in Figure 3-4.

Turbulence measurements were made at various positions in the far wake of each airfoil; these measurements were made with respect to the rotor plane and centerline. It can be seen from Fig. 3-5 that the relative turbulence intensities are fairly weak. Figure 3-5 also shows that the turbulence intensities aren't laterally uniform; however, by definition, turbulence is three-dimensional. Figure 3-6 illustrates a representative variation of wake turbulence intensities with Reynolds number (based on upstream airfoil chord).

A typical autocorrelation and energy spectral density curve is shown in Fig. 3-7. A listing of integral and micro length scales for the airfoil wakes is contained in Table 3-2.

In Fig. 3-8 the one-dimensional energy spectral density for the inflow turbulence at the rotor plane is compared to an isotropic turbulence spectrum obtained from classical turbulence theory. From Hinze [10], the isotropic spectral density corresponding to an exponential velocity correlation is,

$$\frac{U\phi_{uu}}{u'^2 L} = 4 \left\{ 1 + \left[\frac{2\pi f L}{U} \right]^2 \right\}^{-1}. \tag{3.3}$$

For low frequencies, the experimental data shows that the turbulence is clearly nonisotropic. At high frequencies the turbulence approaches isotropy. This behavior has interesting implications concerning the validity of using isotropic turbulence spectrum formulas in low frequency broadband noise prediction schemes.

3.4 Acoustics

After the turbulence measurements were performed, two blades were mounted on the rotor system and operated at the conditions indicated in Table 3-1, with and without an upstream airfoil present. Acoustic measurements were then taken. Typical sound pressure spectra (25 Hz bandwidth) are shown in Fig. 3-9. The microphone was in the on-axis position, 132 cm above the rotor plane.

Background noise measurements with the blades off, were also performed. Sample background sound spectra are shown in Fig. 3-10. For all conditions tested, the background peak sound pressure level was approximately 10 dB lower than the corresponding blade-on configuration. So the assumption of mutual incoherence between the background noise and the turbulence induced noise, and the large dB difference between the background noise and turbulence induced noise, implies that the turbulence induced noise is measured without background contamination.

Acoustic data presented in subsequent plots are 25 Hz bandwidth data, unless otherwise specified (e.g., spectral densities). Also, all acoustic data are referenced to 20 μPa.

4. ANALYSIS OF EXPERIMENTAL RESULTS

In this section, the effects of various rotor performance parameters and type of inflow turbulence on the rotor low frequency broadband noise will be presented and discussed. Comparisons with a noise prediction scheme will also be made. The goal here is to obtain an overall picture of how the rotor broadband noise varies for a variety of initial turbulence states and rotor operating conditions. The main body of the analysis is presented as graphs which show the relationship between a parameter of interest and the measured rotor noise. Empirical scaling laws will not be discussed as they have been exhaustively treated by Aravamudan and Harris [1] and Humbad and Harris [2]. Comparison of experimental acoustic data with a simple broadband noise prediction scheme will provide a test of the validity of the isotropic inflow turbulence assumption which pervades current acoustic analyses.

4.1 Duration of Rotor Blade-Upstream Airfoil Wake Interaction

Because of different upstream airfoil angles of attack and variations of wake geometry for each of the different test cases, the model rotor blades spent different amounts of time in different wakes for a given set of rotor performance parameters. Figure 4-1 shows the effect of blade interaction time (intermittancy) on measured peak sound pressure levels. The intermittancy of the blade-wake interaction was calculated by considering the envelope of the wake and the blade flapping angle, i.e.,

simple geometry. The wake geometry was calculated using a turbulence eddy viscosity (mixing length or Prandtl's hypothesis) model. The rotor blade flapping angle, as a function of azimuth, was calculated using the results of Gessow and Myers [11]. A zero time of interaction corresponds to when the rotor is completely out of the wake. Figure 4-1 was used to correct the subsequent wake-blade SPL data so that plotted SPL values correspond to the rotor blade being in the wake for all azimuth angles. The maximum correction derived this way was 2 dB.

4.2 Rotor Tip Mach Number Effects

Tip Mach number effects on the turbulence induced low frequency broadband noise were investigated by keeping the rotor advance ratio and mean loading constant at $\mu = 0.3$ and $C_T/\sigma = 0.073$, respectively, and varying the rotor rpm. The performance calculations show that the rotor tip path plane is constant for these conditions (note: $\alpha_{shaft} = 0°$).

Figure 4-2 shows the effect of rotor blade tip Mach number on the peak SPL for various upstream conditions. The data is consistent with a sixth power Mach number scaling law. Higher inflow turbulence levels naturally produced higher peak SPL. The high tip Mach number (0.29, 0.39) data were obtained at an advance ratio of 0.1 because of physical limitations of the wind tunnel and rotor system. The data was then corrected to correspond to an advance ratio of 0.3 using the results of Humbad and Harris [2].

4.3 Rotor Advance Ratio Effects

Figure 4-3 shows the effect of rotor advance ratio on the peak SPL. The tip Mach number and rotor loading was kept constant at 0.2 and 0.073, respectively. The advance ratio was varied by changing the wind tunnel speed. This figure shows that the advance ratio (in the range tested) has no strong effect on the peak SPL. Since the relative turbulence intensity decreases with Reynolds number, and the advancing rotor blade tip speed is increased by a factor $1 + \mu$, this result seems plausible. Tip path plane effects could also be significant since our calculations show that the blade flapping changes with the advance ratio.

This advance ratio data complements the corresponding data of Humbad and Harris [2]; their results show that for low advance ratios the sound pressure level increases with advance ratio. The present data is for high advance ratios.

4.4 The Effect of Rotor Mean Thrust

The rotor steady loading was varied by adjusting the collective pitch of the rotor blades, and keeping the blade tip Mach number at 0.16 and the advance ratio at 0.3. It should be kept in mind that the instantaneous blade loading varies as a function of azimuth angle. Figure 4-4 shows that the rotor loading strongly influences the measured sound pressure levels. This loading effect may be due to increased blade flapping velocities and acceleration due to increased mean loading. Leverton and Pollard [12] postulate that increased inflow velocities, due to thrust, may be the cause. Humbad and Harris [2] conducted some experiments on a model rotor to see if the rotor tip path plane and

inflow velocity had any effect on the sound pressure levels; they found that the tip path plane and inflow velocity had little effect.

Another possible cause of SPL variation with rotor thrust is inflow turbulence distortion by the rotor mean thrust. It can be visualized that the rotor flow field stretches and rotates vortex filaments of the initial inflow turbulence, causing additional turbulence production.

4.5 Turbulence Effects

One feature of the present investigation is that initially, the rotor inflow turbulence is of shear layer type and is nonisotropic. Generally, any flow with a mean velocity can't be isotropic. Some characteristics of the effect that the type of inflow turbulence makes on the peak SPL, have already been illustrated, along with the effect of some rotor performance parameters. Figure 4-5 shows that the effect of a characteristic turbulence velocity intensity on the peak SPL is like a velocity squared power law. Figure 4-6 shows how the peak SPL varies with a Strouhal type frequency (constructed from variables of the aeroacoustic problem), $\frac{u'}{L\omega_{pk}}$, where u' is the turbulence rms velocity, ω_{pk} is the acoustic frequency at the peak sound pressure level, and L is the turbulence integral length scale. The figure also shows that the Strouhal relationship depends on the rotor tip Mach number.

To gain some furthur insight on the effect that initial turbulence nonisotropy has on low frequency broadband noise, the experimental acoustic data is compared to a theoretical noise prediction scheme which utilizes a isotropic turbulence spectrum. This is discussed in the following section.

4.5.1 Comparison of Experimental Acoustic Results with a Noise Prediction Scheme Which Utilizes an Isotropic Turbulence Model

Starting from the acoustic result of Morfey and Tanna [13], a simple noise prediction scheme for rotor braodband noise due to incident turbulence, is developed in Appendix A. Acoustically, the rotor blade is represented as a rotating point force. Strictly speaking, this type of representation is correct only if the acoustic wavelength is greater than a typical source dimension, so that the blade surface can be represented as a distribution of dipoles which are all in phase. More sophisticated noise prediction schemes are available, but because of its simplicity, the Appendix A scheme will be used to compare theory with the experimental data.

The isotropic spectrum used for comparison purposes is (Batchelor [14]),

$$\Phi_{22}(k) = \frac{2u'^2}{\pi^2 L} \frac{k_1^2 + k_3^2}{(L^{-2} + k^2)^3} \qquad (4.1)$$

where, $k^2 = k_1^2 + k_3^2$. The values of the intensity u' and the length scale L were obtained from our experiments. The velocity intensity used was the maximum intensity measured; the length scale used was measured in the rotor plane at a distance of 18 cm in front (upstream) of the rotor centerline.

Figure 4-7 shows how the theoretically predicted acoustics, using Eq. (4.1), compares with the experimental data. In general, the agreement is good except for some frequencies where the point force assumption is violated. The agreement for peak sound pressure levels is certainly within 5 dB, which George and Chou [7] state as an acceptable acoustic error. It appears that the nonisotrophy of the initial inflow turbulence does not effect the validity of using an isotropic turbulence assumption in low frequency broadband noise prediction schemes. While the physics of isotropic and nonisotropic turbulence are quite different, it appears that in the context of rotor broadband noise, this difference isn't too significant.

Figure 4-8 shows how the noise prediction scheme is unable to predict the effect of rotor mean loading changes on the acoustics. This implies that either the acoustic model itself is incorrect or the turbulence gust loading is modeled incorrectly.

4.6 Comments

A comparison of a simple theoretical distortion model (Williams and Harris [15]) with experimental model rotor data indicates that a single shear type turbulence distortion, as a function of rotor mean loading, cannot totally explain observed increases in sound pressure with increased rotor mean thrust. Other, more robust, phenomena occur when the rotor mean thrust increases, e.g., increased blade flapping velocities and acceleration, and increased rotor inflow velocity. But this doesn't lessen the utility of the inflow turbulence distortion concept.

Conceptually, the idea of inflow turbulence distortion is an attractive one, since in real rotor flows the turbulence is constantly being distorted. More analysis is needed to determine the full utility of this concept in explaining turbulence related noise from helicopter rotors. Specifically, expressions linking the rotor mean aerodynamics to the evolution of an initial turbulence state need to be developed[15].

5. CONCLUSIONS

Measurements were taken to gain some understanding of how shear layer type inflow turbulence would effect the low frequency broadband noise of a model helicopter rotor. The measurements and the one dimensional energy spectral density indicated that the upstream airfoil wake turbulence was nonisotropic, but it approached isotropy at high wavenumbers. Turbulence measurements also indicated that the wake turbulence was weak. The effect of the inflow turbulence intensity on the peak sound pressure level follows an intensity velocity squared scaling law.

One important fact that was illustrated by the turbulence measurements, was that there exist a number of length scales and turbulence intensities which could be measured in the airfoil wake depending on the position at which the measurements were taken. How well experimental data compares with theory or some noise prediction scheme clearly depends on the choice of measured length scales and intensities utilized in the prediction scheme. There is some arbitrariness in this choice and previous investigators have not pointed this out. Of course, some choice must be made, and that

choice may depend on the experimental study being done. In this paper, the velocity intensity used in the prediction scheme was the maximum intensity measured; the length scale was measured in the rotor plane at a distance of 18 cm in front of the rotor centerline. This inherent richness of scales and intensities mimic full-scale rotor phenomena. More theoretical work needs to be done to understand the effect of such flow inhomogeneities on the rotor broadband noise.

The comparison of experimental and theoretical sound pressure power spectral densities indicate that the initial nonisotropy of the inflow turbulence doesn't invalidate the isotropic turbulence assumption made in noise prediction models, as long as measured turbulence intensities and length scales are used. That is, the assumption of a constant turbulence intensity and length scale, and an isotropic turbulence spectrum leads to quite reasonable broadband noise prediction. This is a somewhat surprising result (which may be a fortuitious coincidence) in view of how the rotor aerodynamics can contribute by means of vortex straining, blockage effects, and shed vorticity, to the kinetic energy dynamics of the initial inflow turbulence. Other investigators have pointed out the success of broadband noise prediction schemes for grid generated, isotropic inflow turbulence (George and Chou [7]).

The effect of rotor performance parameters on the low frequency broadband noise due to incident turbulence, follows the scaling laws derived by Humbad and Harris [2]. For the high advance ratios considered here, the observed peak sound pressure levels were found to be relatively independent of the rotor advance ratio. The experimental measurements showed that the relative turbulence intensity decreased with the mean flow Reynolds number, so this observation seems plausible.

For the range of parameters tested, it was found that increasing the rotor mean thrust increased the observed peak sound prssure levels. Previous investigators have not theoretically explained this phenomenon. This problem was treated analytically by Williams and Harris [15].

Conceptually, the idea of inflow turbulence distortion is an attractive one, since in real rotor flows the turbulence is constantly being distorted. More analysis is needed to determine the full utility of this concept in turbulence related noise. The most important analysis needed is one which links the rotor aerodynamics to the evolution of the turbulent flow field.

ACKNOWLEDGEMENTS

This research program was supported in part by NASA Grant NSG - 1583.

REFERENCES

1) Aravamudan, K. S. and Harris, W. L., "Experimental and Theoretical Studies on Model Helicopter Rotor Noise." M.I.T. FDRL Report No. 78-1, 1979.

2) Humbad, N. G. and Harris, W. L., "Effects of Tip Geometry on Model Helicopter Rotor Low Frequency Broadband Noise." M.I.T. FDRL Report No. 81-2, 1981.

3) Paterson, R. W. and Amiet, R. K., "Noise of a Model Helicopter Rotor Due to Ingestion of Turbulence," NASA CR-3212, 1979.

4) Homicz, G. F. and George, A. R., "Broadband and Discrete Frequency Radiation from Subsonic Rotors." Journal of Sound and Vibration, 36, p. 110, 1974.

5) George, A. R. and Kim, Y. N., "High Frequency Broadband Rotor Noise." AIAA Journal, Vol. 15, 1. 538, 1977.

6) Amiet, R. K., "Noise Produced by Turbulent Flow Into a Propeller or Helicopter Rotor." AIAA Journal, Vol. 15 (3), 1977.

7) George, A. R. and Chou, S. T., "Comparison of Broadband Noise Mechanisms, Analyses, and Experiments on Helicopters, Propellers, and Wind Turbines." AIAA Paper, AIAA-83-0690, 1983.

8) Bendat, J. S. and Piersol, A. G., Random Data Analysis and Measurement Procedures, Wiley-Interscience, 1971.

9) Widnall, S. E., Harris, W. L., Lee, A., and Drees, H. M., "The Development of Experimental Techniques for the Study of Helicopter Rotor Noise." NASA CR-137684, 1974.

10) Hinze, J.O., Turbulence, Second Edition, McGraw-Hill, N.Y., 1975.

11) Gessow, A. and Myers, G. C., Aerodynamics of the Helicopter, Frederick Ungar Publishing Co., N.Y., 1952.

12) Leverton, J. W. and Pollard, J. S., "Comparison of the Overall and Broadband Noise Characteristics of Full Scale and Model Helicopter Rotors." Journal of Sound and Vib., 30(2), p. 135, 1973

13) Morfey, C. L. and Tanna, H. K., "Sound Radiation from a Point Source in Circular Motion." Journal of Sound and Vib., 15, p 325, 1971.

14) Batchelor, G. K., The Theory of Homogeneous Turbulence, Cambridge University Press, N.Y. 1953.

15) Williams, M., and Harris, W. L., "A Theoretical Analysis of the Effect of Thrust Reated Turbulence Distortion on Helicopter Rotor Low Frequency Broadband Noise." Paper No. 17, Proceeding of the Tenth European Rotorcraft Forum, The Hague, The Netherland, August 28-31, 1984.

16) Mugridge, B. D., "Gust Loading on a Thin Airfoil." Aero. Quart., 22, pt. 3, p. 301, 1971.

APPENDIX A

A SIMPLE BROADBAND NOISE PREDICTION SCHEME

Starting form the acoustic result of Morfey and Tanna [13], a simple noise prediction scheme for rotor broadband noise due to incident turbulence is developed. This scheme is valid for on-axis observer location.

Formulation of the Problem

The theory presented in this Appendix is based on the idea that turbulence velocity fluctuations cause corresponding blade lift fluctuations. This phenomena will be modelled as a single point force undergoing uniform ciruclar motion. The point force approximation is strictly valid only for acoustic wavelengths greater than a typical source dimension (blade chord or span), therefore, care must be taken when interpreting the theoretical results for high frequencies. The strength of the point force will be calculated by treating the turbulence as a frozen, covected three-dimensional gust and using unsteady, compressible thin airfoil theory with a strip approximation. Blade to blade correlation isn't accounted for in the present treatment. The turbulence induced unsteady loading on different rotor blades is assumed to be uncorrelated. The turbulence is assumed to be homogeneous and all random processes are assumed to be stationary.

Development of the Model

Morfey and Tanna [13] developed an expression for the sound pressure spectral density S_{pp} due to a time varying point force in uniform rotaion about a circle. The equation is,

$$S_{pp}(\omega) = \frac{\cos^2\theta}{(4\pi ar)^2}\left\{\omega^2 \mathcal{J}_{LL}(\omega) + \frac{\omega^4 M^2 \sin^2\theta}{4}\frac{d^2\mathcal{J}_{LL}}{d\omega^2} + \frac{\omega^6 M^4 \sin^4\theta}{64}\frac{d^4\mathcal{J}_{LL}}{d\omega^4}\right\} + 0\frac{\Omega^2}{\omega^2} \tag{A.1}$$

Equation (A.1) neglects blade drag and assumes that the blade Mach number is less than one. For details of the developement of Eq. (A.1) see Morfey and Tanna [13].

To calculate the lift spectral density S_{LL}, Taylor's hypothesis for weak turbulence is used. The turbulence upwash field may be considered as frozen gusts. The gust is assumed to be three-dimensional and the rotor blade is modelled as a thin two-dimensional airfoil at a distance r_o from the rotor axis.

From Aravamudan and Harris [1] the lift spectral density is,

$$S_{LL}(\omega) = \frac{1}{Q}\int_{-\infty}^{\infty}\int \left|K\left(\frac{-\omega}{Q},k_z\right)\right|^2 \Phi_{vv}\left(\frac{-\omega}{Q},k_y,k_z\right)dk_y dk_z \tag{A.2}$$

In the general case, the energy tensor Φ_{22} must be transformed to local airfoil coordinates from the coordinate system in which the turbulence was originally measured or derived. This is done by the usual tensor transformation rules.

To complete the determination of S_{LL}, it is necessary to select a specific lift transfew function K and an upwash energy spectral density Φ_{vv}. For K, a low and high frequency approximation to the compressible Sears function will be used. For low frequencies (Amiet [6]),

$$\frac{1}{CL}\frac{|K(k_x,k_z)|^2}{|F(k_x,k_z)|^2} = \frac{|S(\sigma_1/\beta^2)|^2}{\beta^2}\left\{J_o{}^2\left(\frac{M^2\sigma_1}{\beta^2}\right)+ J_1{}^2\left(\frac{M^2\sigma_1}{\beta^2}\right)\right\},$$

$$\text{for } \frac{M\sigma_1}{\beta^2} < 1, \tag{A.3}$$

and for high frequencies,

$$\frac{1}{CL}\frac{|K(k_x,k_z)|^2}{|F(k_x,k_z)|^2} = (\pi^2\sigma_1{}^2M)^{-1}$$

$$\text{for } \frac{M\sigma_1}{\beta^2} > 1 \tag{A.4}$$

where, $CL = (\pi\rho Qcb)^2$, $\sigma_1 = k_xC/z$, $F(k_x,k_z)$ is effectively a strip theory correction factor. From Mugridge [16],

$$|F(k_x,k_z)|^2 = \frac{\sigma_1{}^2 + 2/\pi^2}{\sigma_o^2+\sigma_3^2+\frac{2}{\pi^2}} \quad ; \quad \sigma_i = k_i\,C/z \tag{A.5}$$

The analysis of Mugridge showed that Eq. (A.5) multiplied by a Sears function, tends to overestimate the mean square lift of an infinite span airfoil encountering a three-dimensional gust for values of σ_1,σ_2 greater than 2.

For isotropic turbulence and an exponential correlation function, the upwash spectral density can be written as (Batchelor [14]),

$$\Phi_{vv} = \frac{2u'^2}{\pi^2L}\frac{(k_x{}^2 + k_z{}^2)}{L^{-2} + k^2)^3} \tag{A.6}$$

where, $k^2 = k_x{}^2 + k_y{}^2 + k_z{}^2$.

There is no special significance in the choice of the gust lift transfer function or upwash spectral density other than that they result in a simple expression for the lift spectral density S_{LL}.

Substituting Eqs. (A.3) or (A.4) and (A.6) into Eq. (A.2) and integrating,

$$S_{LL}(\omega) = \frac{3\pi}{L} u'^2 Q(\rho b)^2 \tilde{A}(k_x) \left\{\sigma_1^2 + \frac{2}{\pi^2}\right\}\left\{k_x^2 + L^{-2}\right\}^{-2} \cdot I(k_x, \frac{L}{C}) \qquad (A.7)$$

where, depending on the frequency range of interest, $\tilde{A}(k_x)$ is given by Eq. (A.3) or A.4). Define, $A = k_x^2/(k_x^2 + L^{-2})$, $B = \dfrac{k_x^2 + 8/\pi^2 C^2}{k_x^2 + L^{-2}}$, Then $I(k_x, \frac{L}{C})$

$$\equiv \frac{2}{\sqrt{B(1-B)}}\left\{A - \frac{B(1-2A)}{1-B} + \frac{B^2(A-1)}{(1-B)^2}\right\}\tan^{-1}\sqrt{\frac{1-B}{B}} + \frac{4-10A}{3(1-B)} - \frac{2B(A-1)}{(1-B)^2}$$

for $\dfrac{L^2}{C^2} < \dfrac{\pi^2}{8}$. And

$I(k_x, \frac{L}{C}) \equiv$

$$\frac{2}{\sqrt{B(B-1)}}\left\{A - \frac{B(1-2A)}{1-B} + \frac{B^2(A-1)}{(1-B)^2}\right\}\tanh^{-1}\sqrt{\frac{B-1}{B}} + \frac{4-10A}{3(1-B)} - \frac{2B(A-1)}{(1-B)^2}$$

for $\dfrac{L^2}{C^2} > \dfrac{\pi^2}{8}$. Finally, $I(k_x, \frac{L}{C})$ ▫

$$\frac{4 + 16A}{15}, \quad \text{for } \frac{L^2}{C^2} = \frac{\pi^2}{8} \text{ or } k_x \to \infty .$$

The final result for the sound pressure spectral density is,

$$S_{pp}(\omega) \approx \frac{\cos^2\theta}{(4\pi ar)^2} \frac{Q3\pi u'^2}{L} (\rho b\omega)^2 \tilde{A}(k_x)\left\{\sigma_1^2 + \frac{2}{\pi 2}\right\}\left\{k_x^2 + L^{-2}\right\}^{-2} \cdot I(k_x, \frac{L}{C}) \qquad (A.8)$$

where, $\omega^6 M^4 \sin^4\theta << 1$.

Table 2-1. Upstream Airfoil Dimensions.

Section	Chord	Span
0012	30.5 cm	223.5 cm
1112	38.1	223.5
63A012	38.1	223.5

Table 3.1. Test Matrix.

Advance Ratio	Shaft Rotational Frequency	C_T/σ	Blade Pitch*
0.3	474 rpm	0.073	10 deg
0.3	611	0.073	10
0.3	810	0.073	10
0.3	1046	0.073	10
0.1	1500	0.073	11.7
0.1	2000	0.073	11.7
0.3	810	0.006	6
0.3	810	0.040	8
0.3	810	0.140	14
0.18	810	0.073	10.8
0.23	810	0.073	10.4
0.39	810	0.073	9.4

*Measured at the blade root.

Table 3-2. Turbulence length scales of the upstream airfoil wake measured at x = -18 cm, y = 0, z = -56 cm.

Rotor-upstream airfoil configuration	$Re_{c_{upstream}}$	Longitudinal microscale	Longitudinal integral scale
S-1	2×10^5	0.59 cm	5.8 cm
S-2	2	0.59	3.8
S-3	2	0.66	2.6
S-4	2.5	0.54	1.9
S-5	2.5	0.73	3.6
S-6	2.5	0.62	1.9
S-7	2.5	0.59	3.5

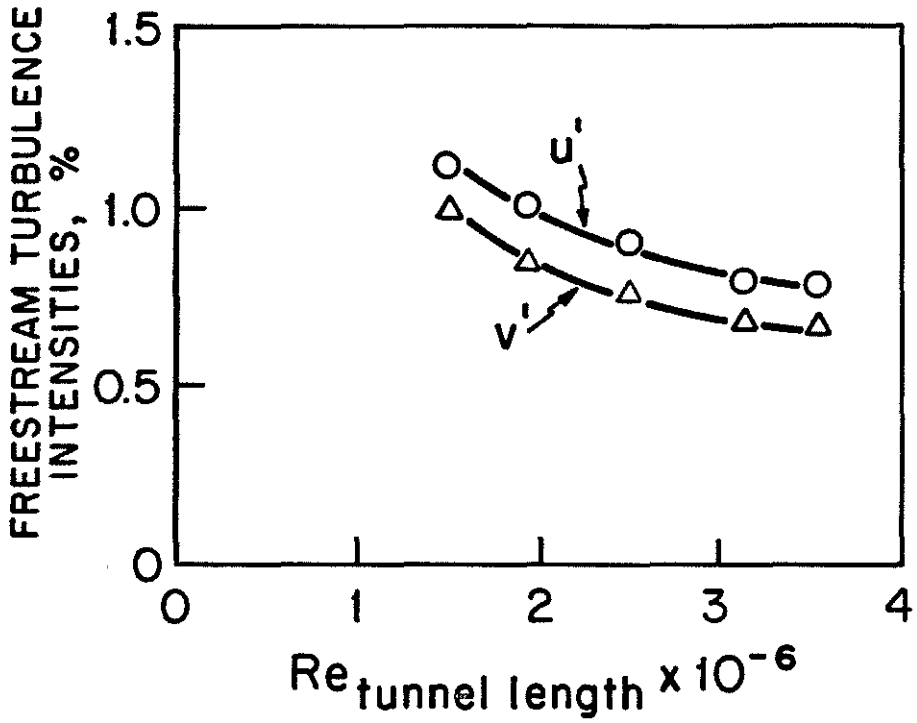

Figure 3-1. Freestream turbulence intensities.

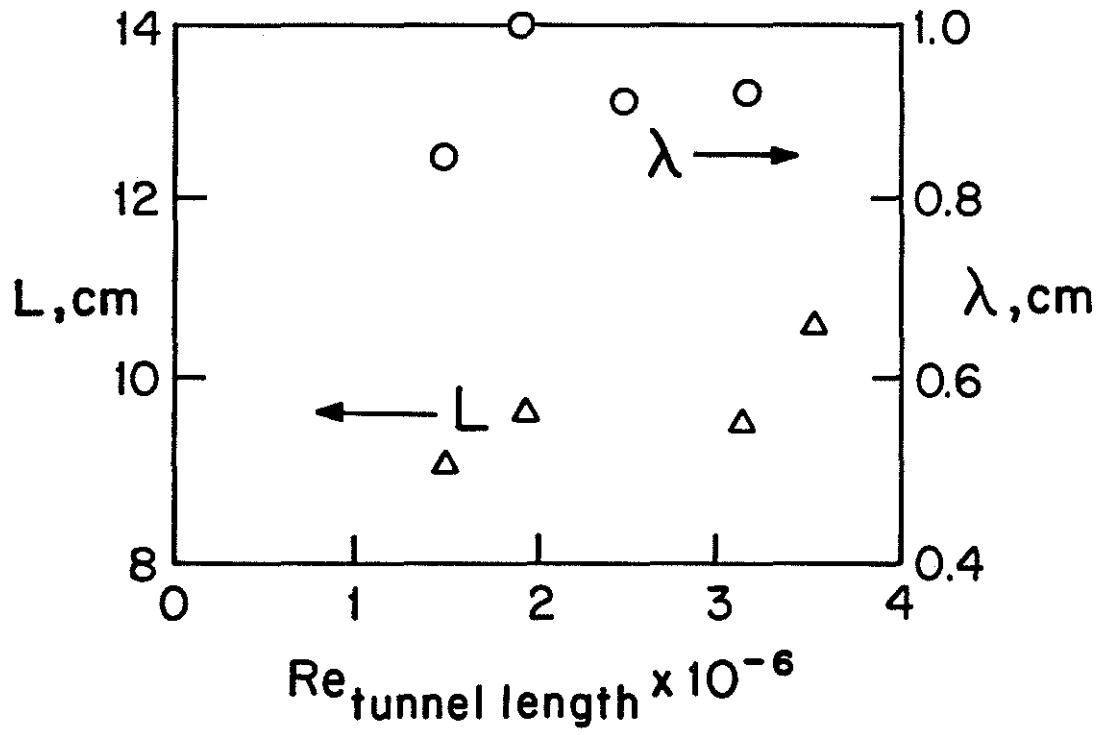

Figure 3-2. Variation of freestream length scales.

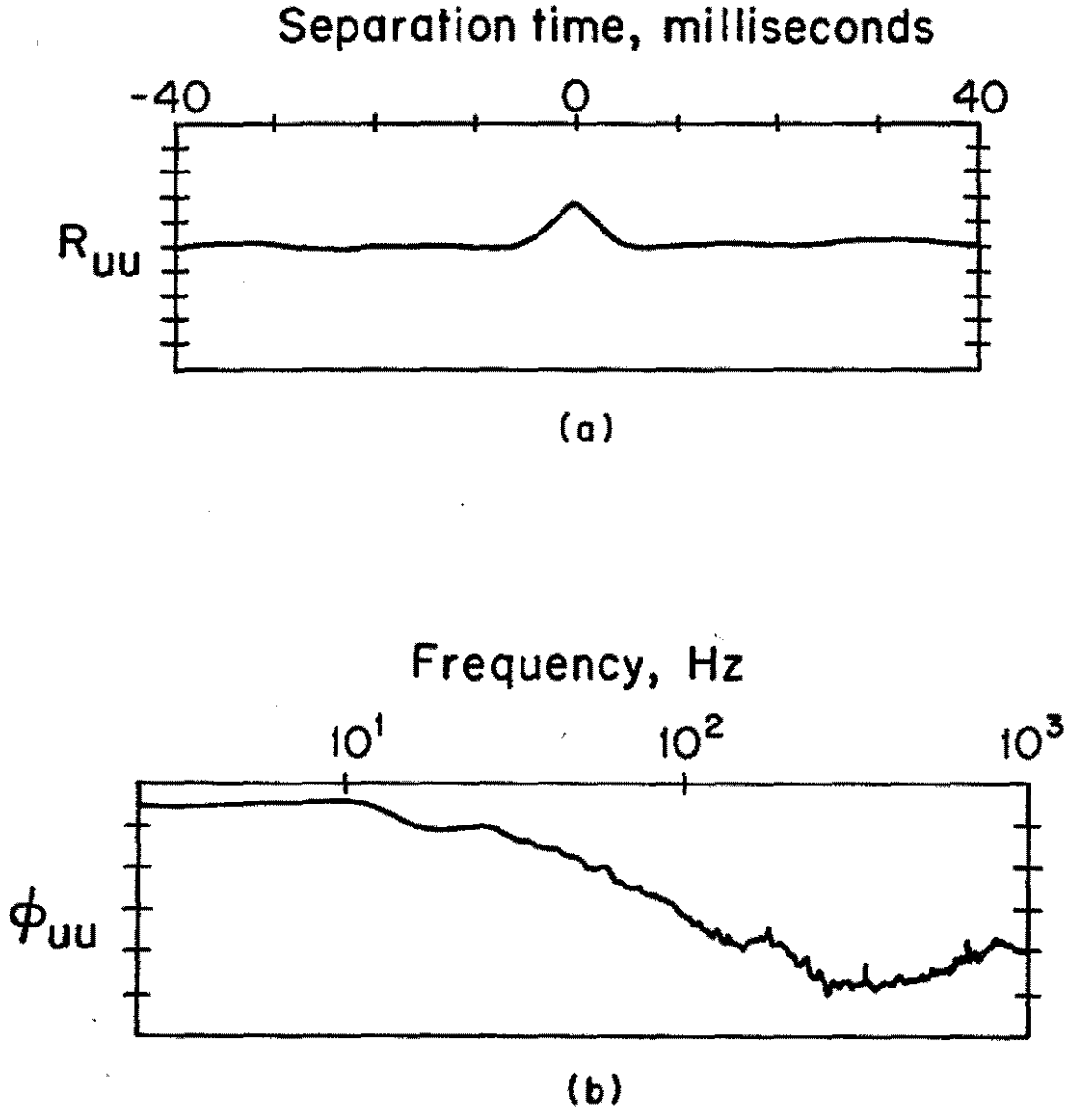

Figure 3-3. Typical freestream autocorrelation curve (a), and one-dimensional energy spectral density curve (b), for Re = 1.5×10^6; arbitrary vertical scales.

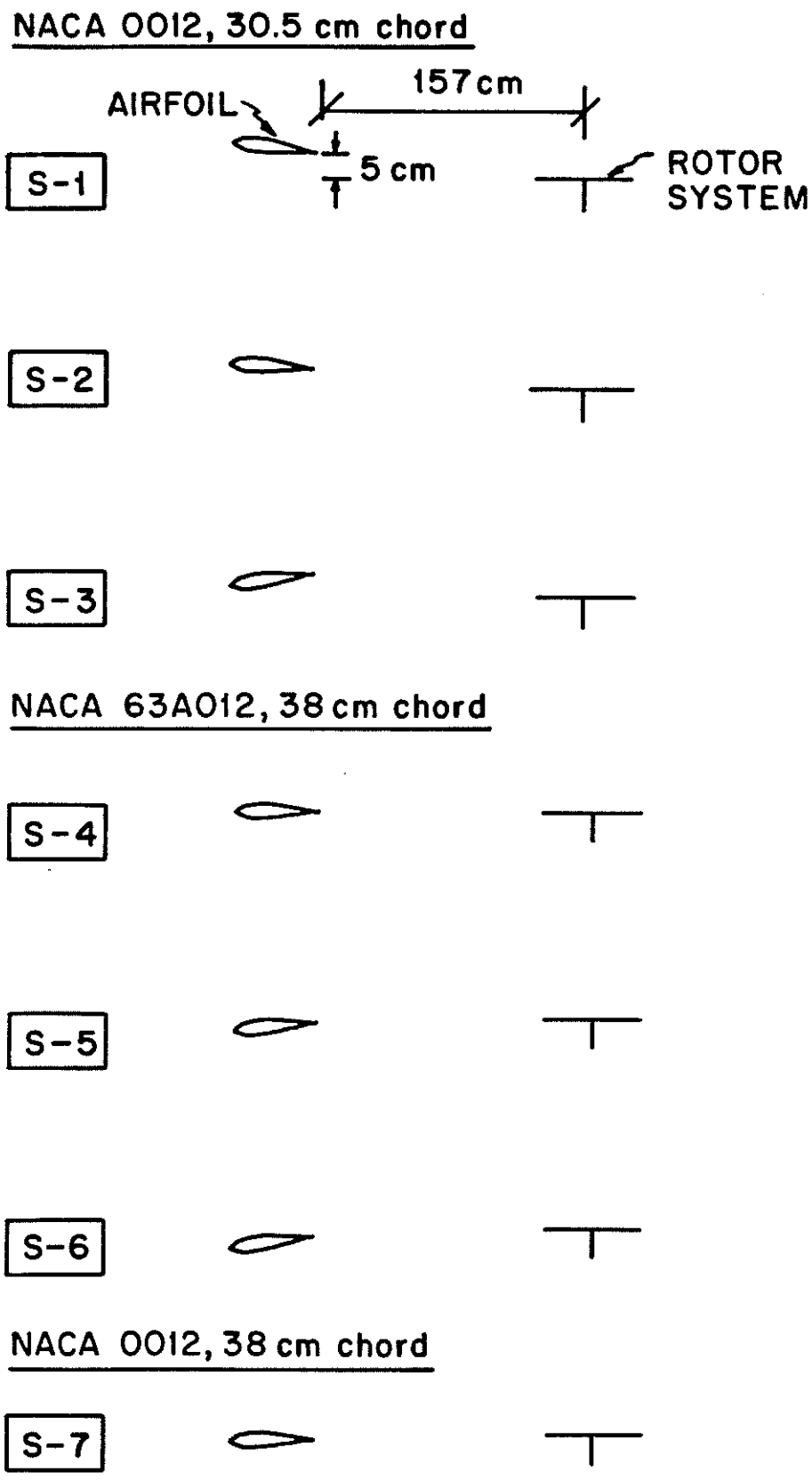

Figure 3-4. Schematic of the upstream airfoil arrangement.

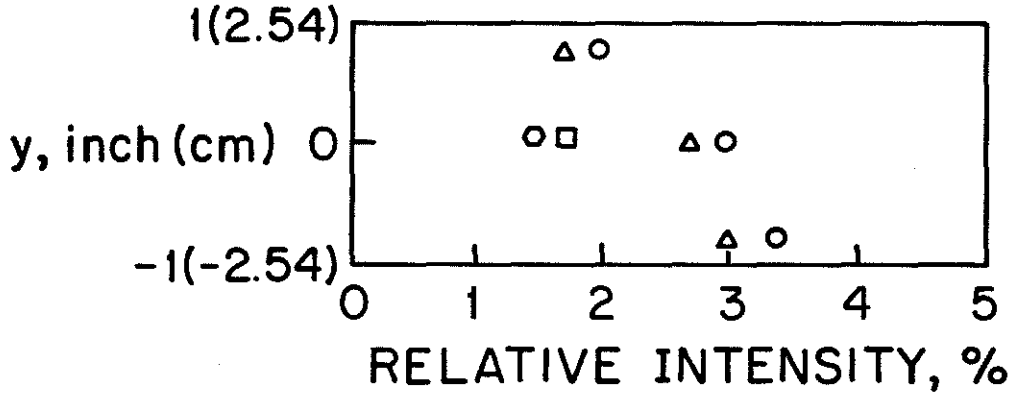

(a) S-1. ○ u/U, △ v/V at (x,z) = (-18,056) cm
□ u/U, ⬡ v/U at (x,z) = (-18,-42)

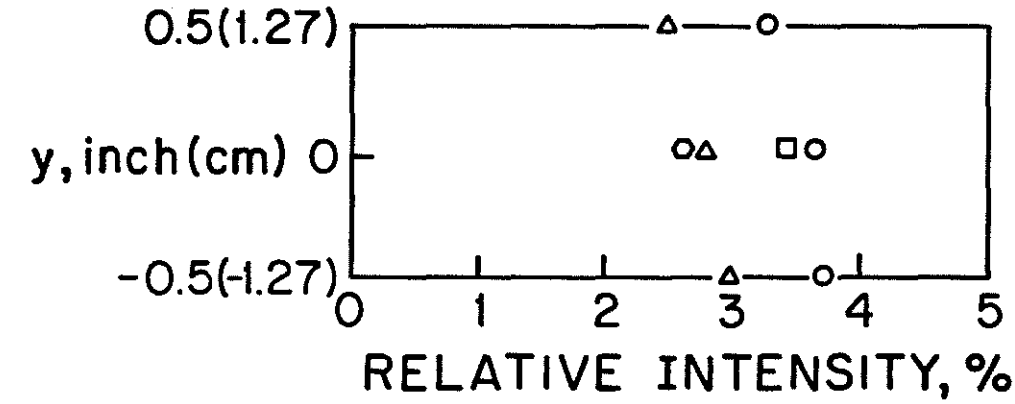

(b) S-2. ○ u/U, △ v/U at (x,Z) = (-18,-56)
□ u/U, ⬡ v/U at (x,z) = (-18,-42)

Figure 3-5. Upstream airfoil wake turbulence intensities.

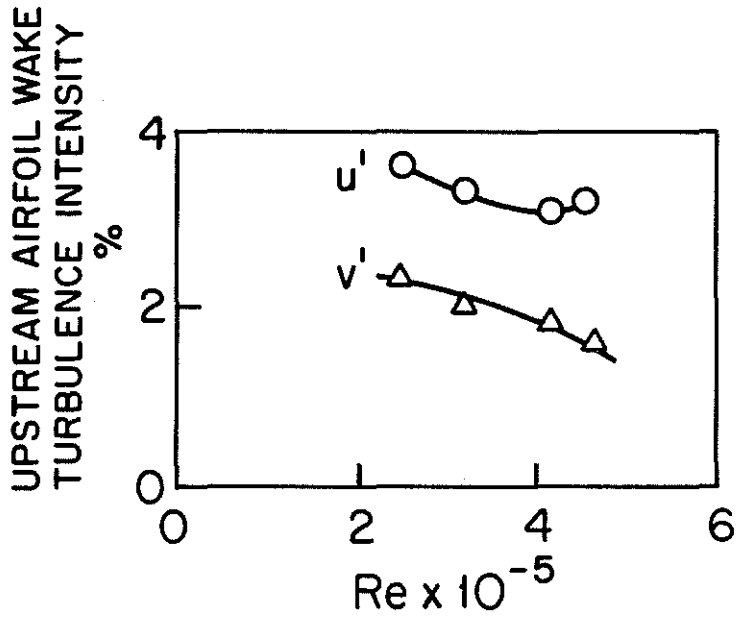

Figure 3-6. Variation of upstream airfoil wake turbulence intensity for S-7.

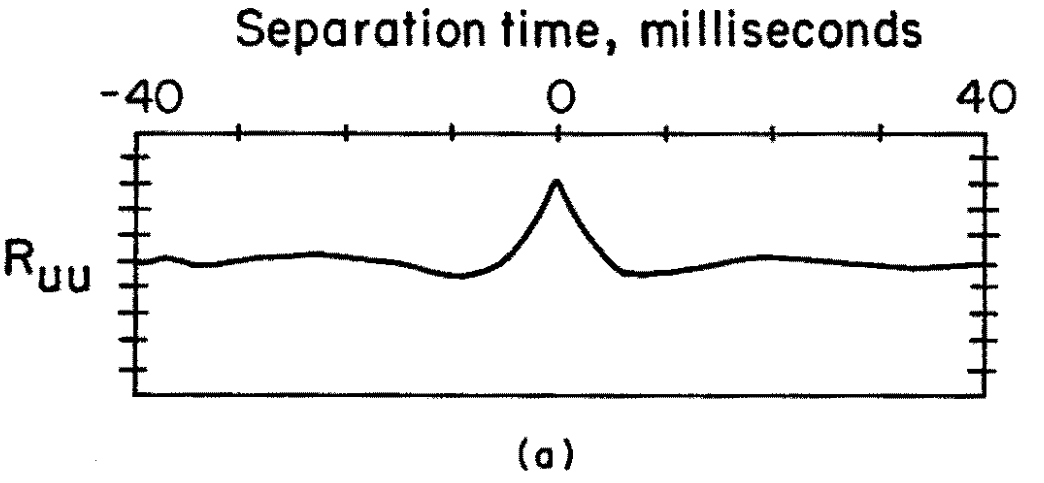

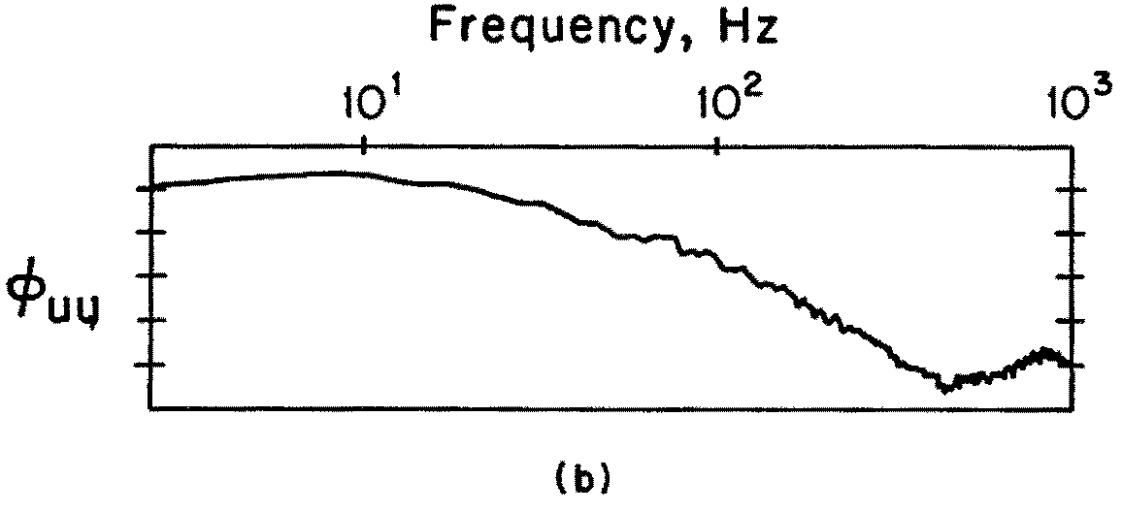

Figure 3-7. Typical upstream airfoil (S-4) wake turbulence auto-correlation curve (a), and one-dimensional energy spectral density curve (b), for Re = 2.5 x 10^5; arbitrary vertical scales.

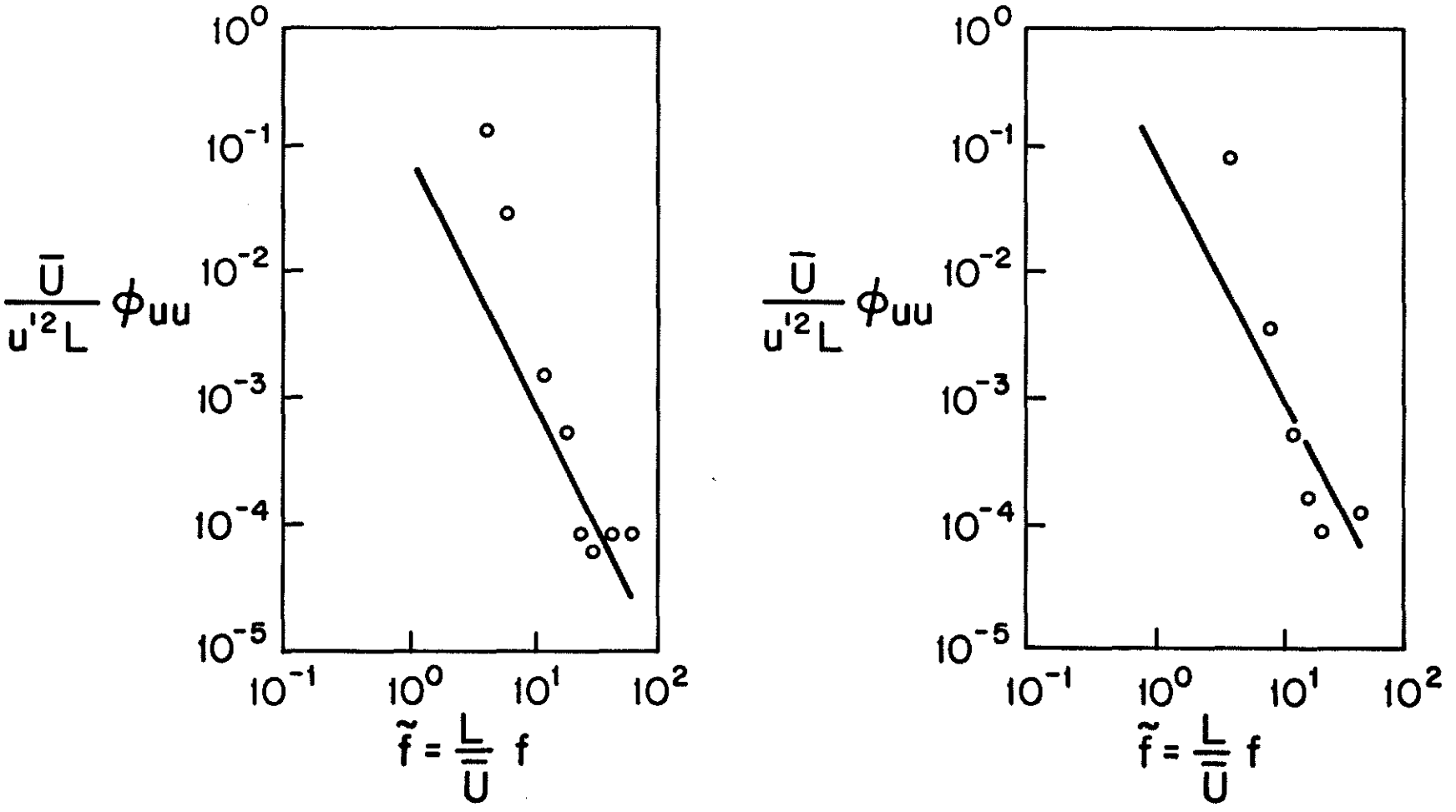

Figure 3-8. Comparison of experimental (O) one-dimensional energy spectral density of the upstream wake to a theoretical isotropic spectrum (—); (x,y,z) = (-18,0,-56) cm.

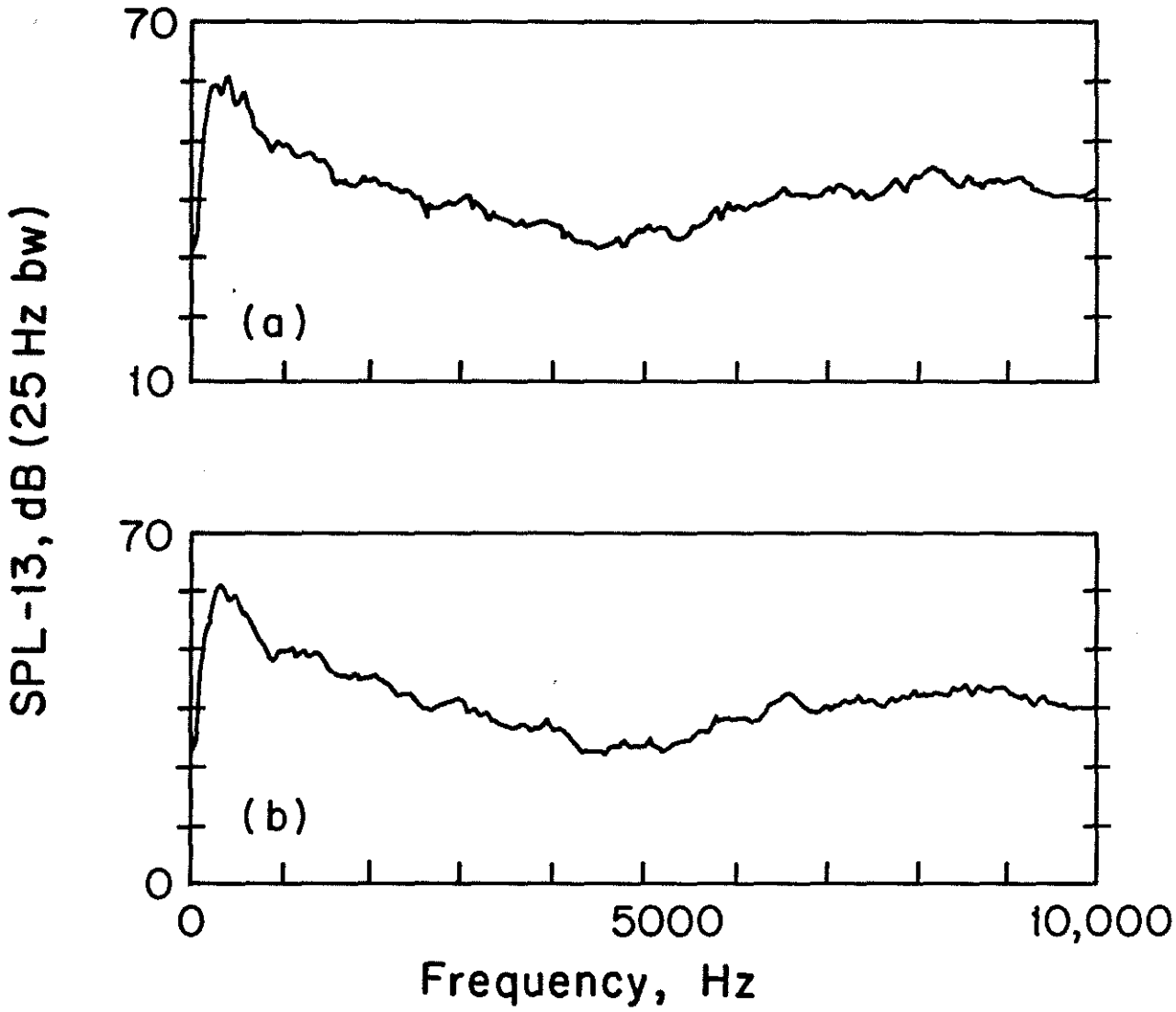

Figure 3-9. Typical sound pressure spectra; microphone in the on-axis position, 132 cm above the rotor plane; tip Mach number = 0.2, μ = 0.3, C_T/σ = 0.073; (a), S-3; (b), S-4.

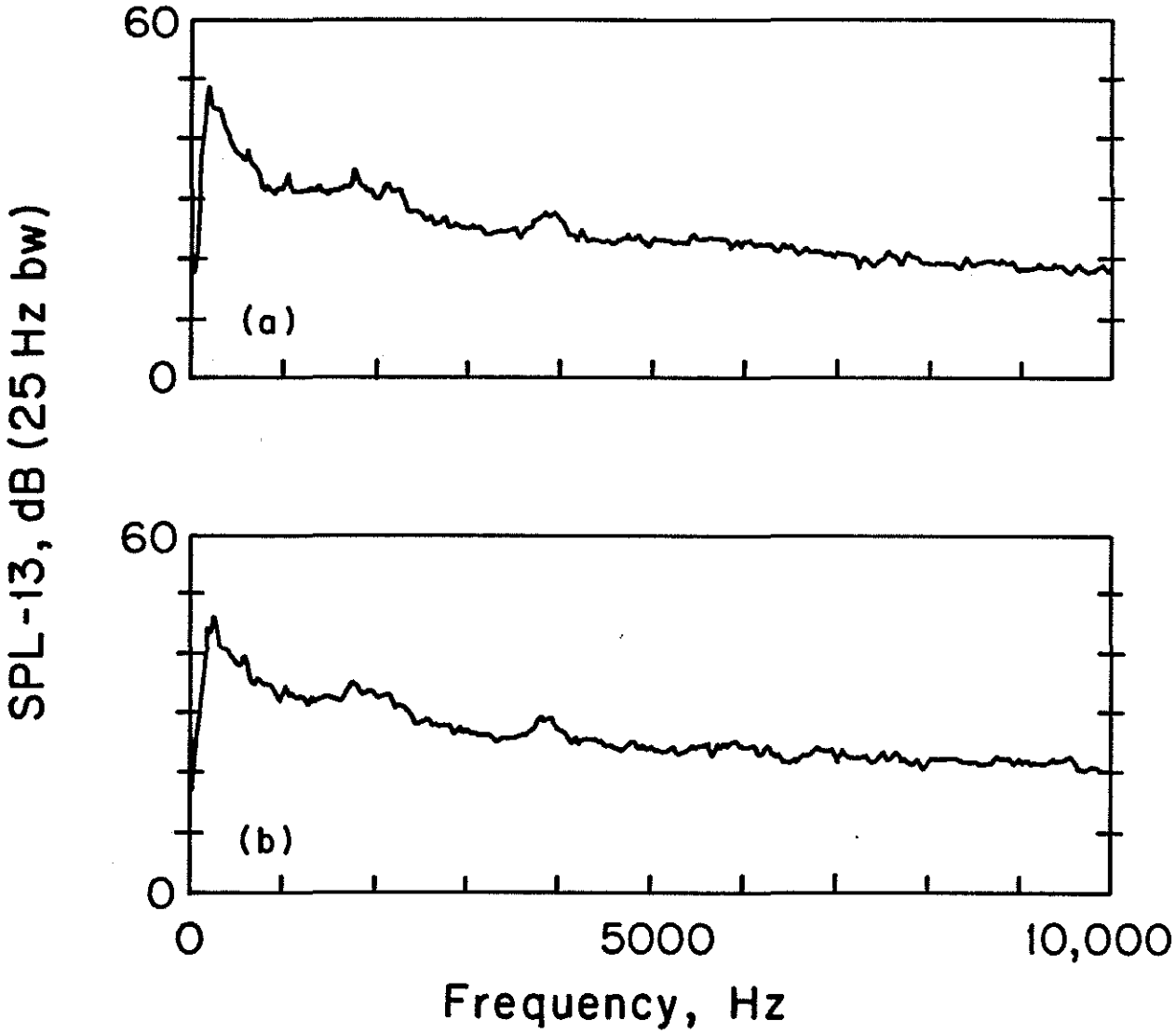

Figure 3-10. Background sound spectra with rotor blades removed; conditions listed in Fig. 3-9; (a), S-3; (b), S-4.

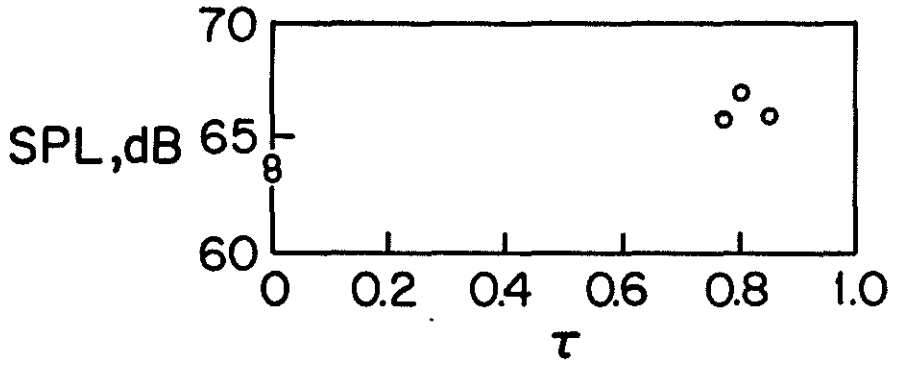

Figure 4-1. Peak SPL variation with duration of blade-upstream airfoil wake interaction

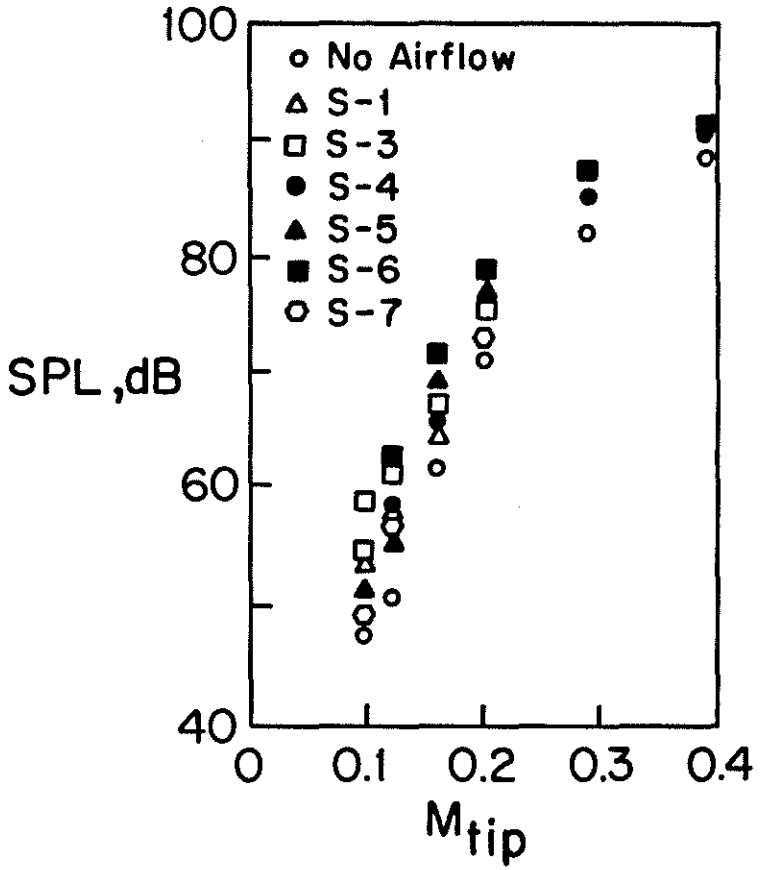

Figure 4-2. Effect of blade tip Mach number on peak SPL for various upstream conditions; $\mu = 0.3$, $C_T/\sigma = 0.073$.

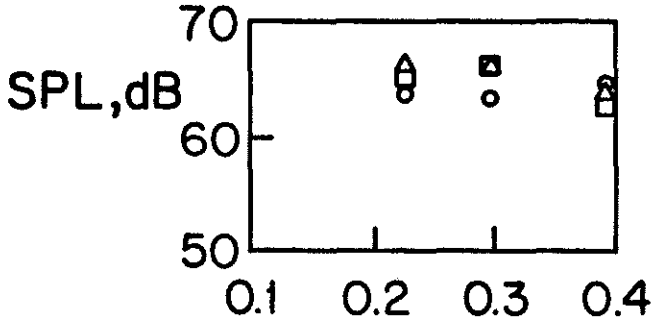

Figure 4-3. Invariance of peak SPL for high advance ratios; ○, clean; △, S-1; □, S-4, M_{tip} = 0.2; C_T/σ = 0.073.

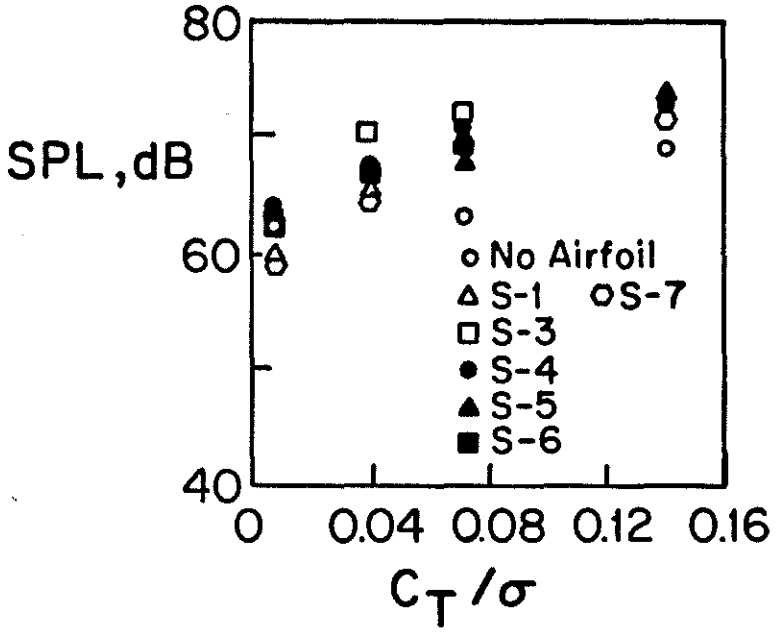

Figure 4-4. Influence of rotor mean loading on peak SPL; M_{tip} = 0.2; μ = 0.3.

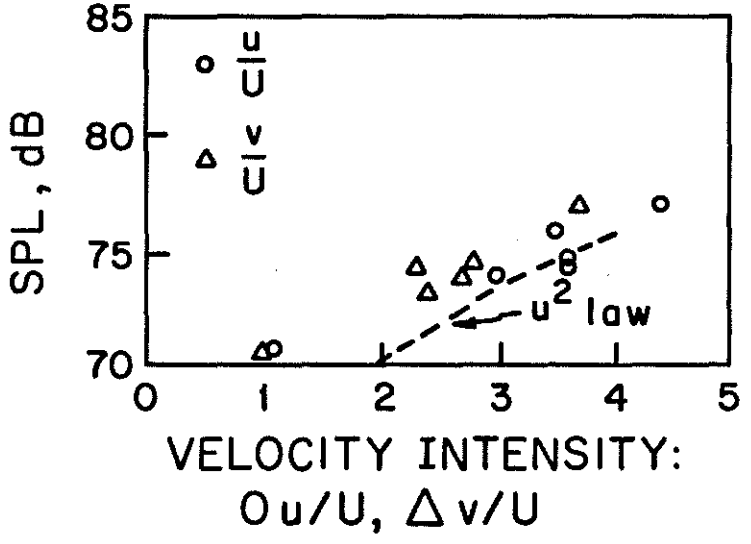

Figure 4-5. Effect of characteristic turbulence velocity on the peak SPL; $M_{tip} = 0.2$; $\mu = 0.3$; $C_T/\sigma = 0.073$.

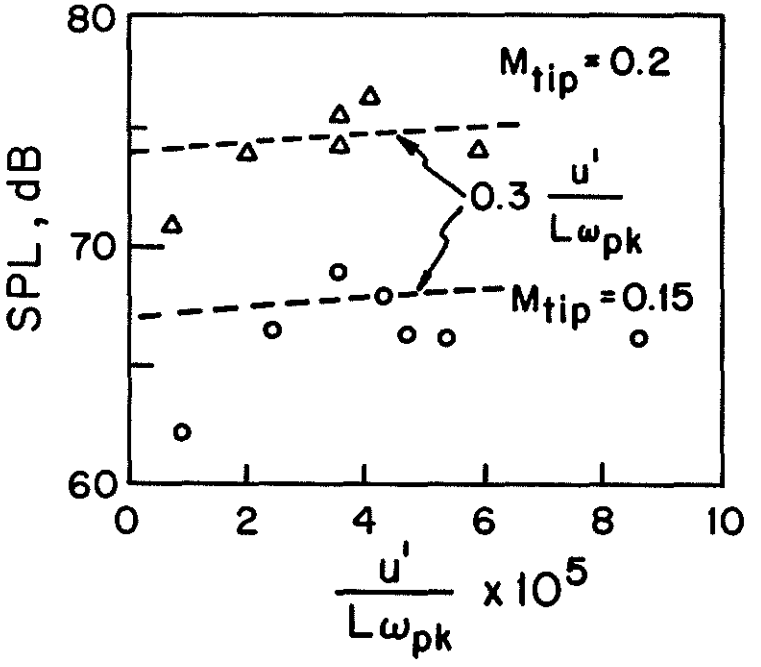

Figure 4-6. Correlation of the non-dimensional frequency $\frac{u'}{L\omega_{pk}}$ with peak SPL.

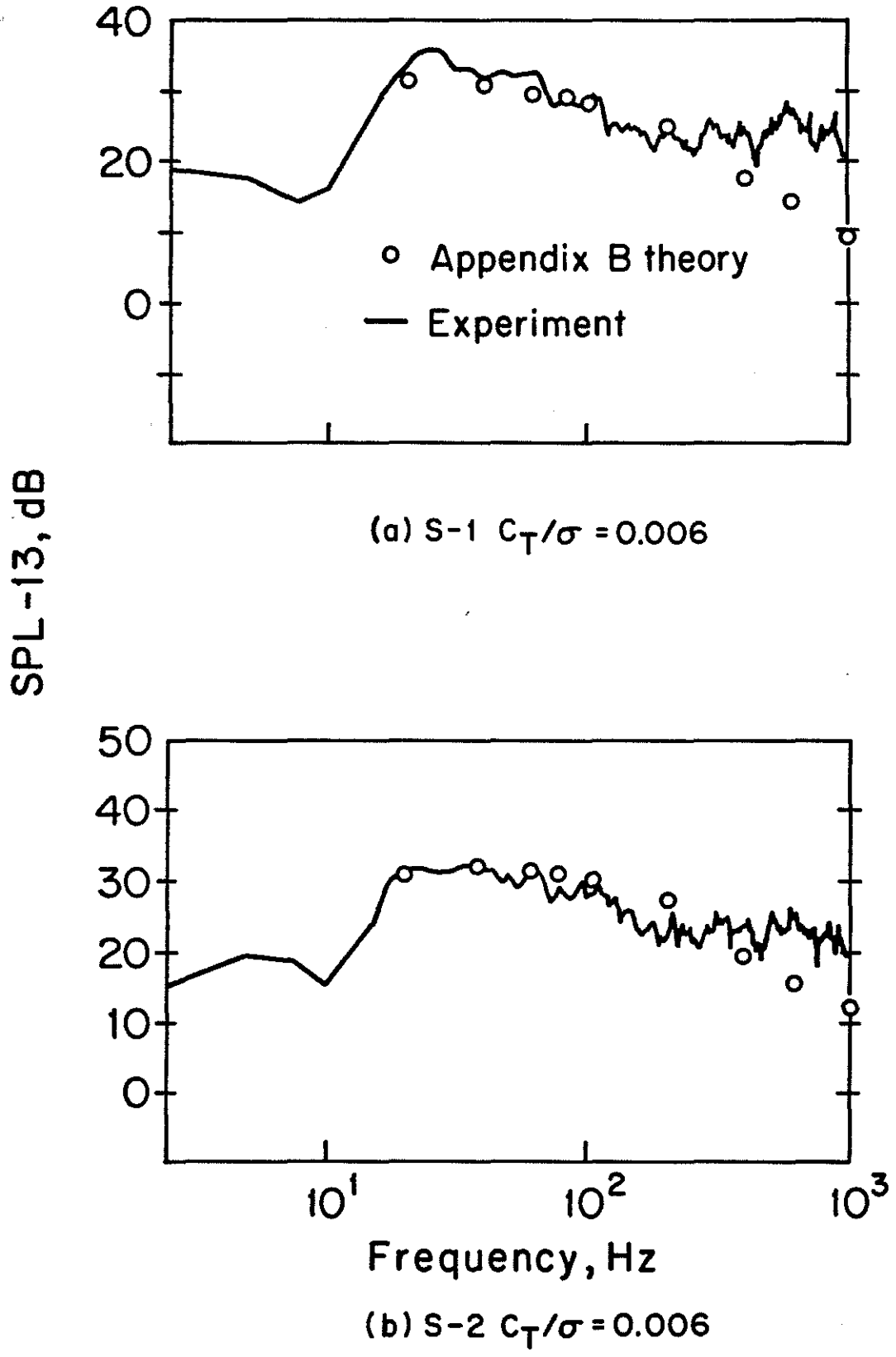

Figure 4-7. Comparison of theoretically predicted sound pressure spectral densities with experimental data; M_{tip} = 0.16; = 0.3.

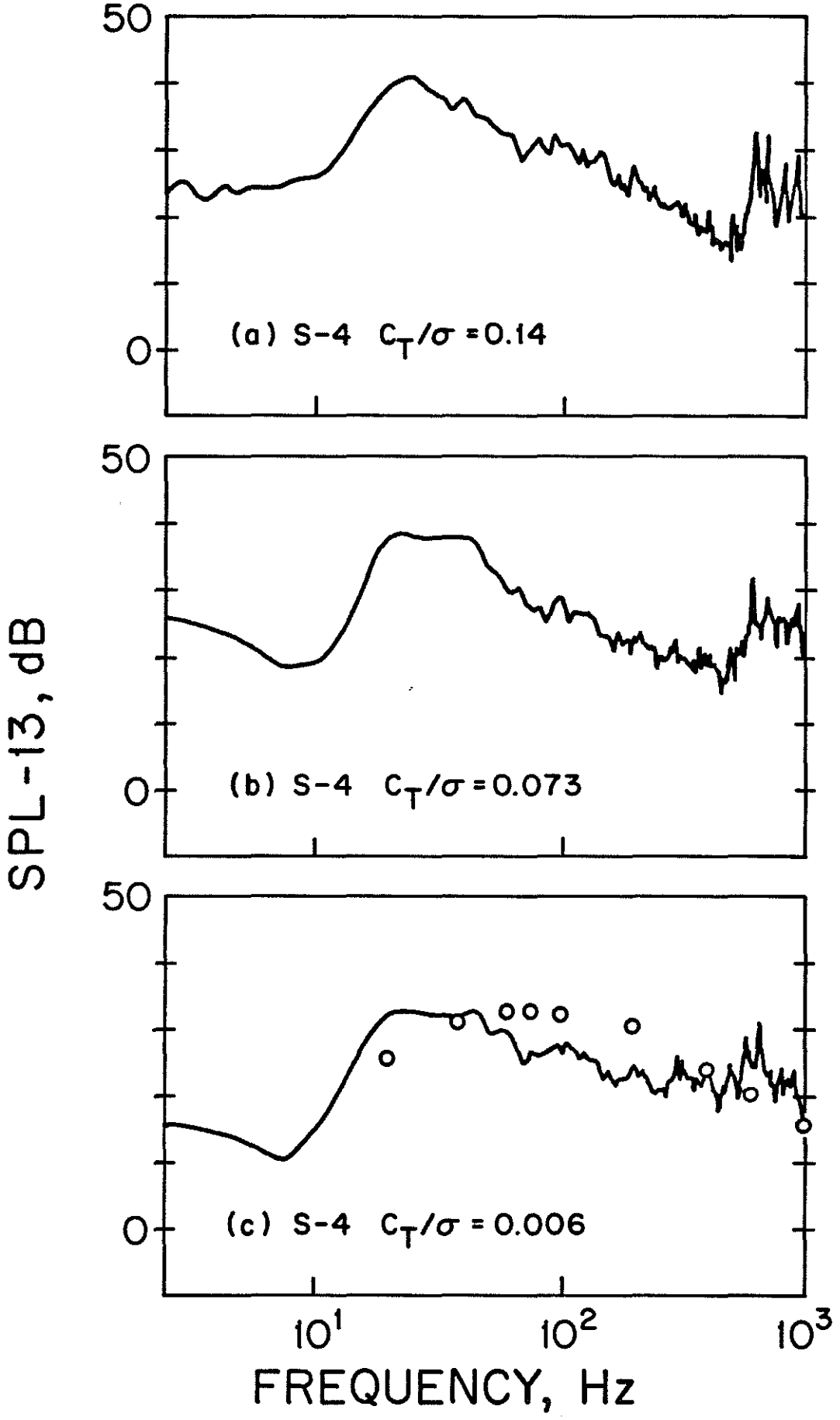

Figure 4-8. The effect of rotor mean loading on the sound pressure spectral density; M_{tip} = 0.16; μ = 0.3.